Journal of Geophysical Research: Space Physics

RESEARCH ARTICLE
10.1029/2018JA025709

**Key Points:**
- We perform a study of intraseasonal variability of nonmigrating tides at ~97-km altitude using the MLS multiyear temperature observations
- Approximately 30- to 60-day periodicities are observed in the amplitudes of wave-3 and wave-4 longitudinal structures
- Intraseasonal variations of the wave-3 and wave-4 structures are found to coincide with the corresponding periodic signatures in rainfall

**Correspondence to:**
G. Liu,
guiping@berkeley.edu

**Citation:**
Liu, G., Janches, D., & Lieberman, R. S. (2018). Intraseasonal variations of nonmigrating tides observed near the mesopause. *Journal of Geophysical Research: Space Physics*, *123*, 9921–9931. https://doi.org/10.1029/2018JA025709

Received 23 MAY 2018
Accepted 8 NOV 2018
Accepted article online 12 NOV 2018
Published online 28 NOV 2018



# Intraseasonal Variations of Nonmigrating Tides Observed Near the Mesopause

**Guiping Liu[1,2], Diego Janches[3], and Ruth S. Lieberman[3]**

[1]Space Sciences Laboratory, University of California, Berkeley, CA, USA, [2]CUA/NASA GSFC, Greenbelt, MD, USA, [3]Heliophysics Science Division, NASA Goddard Space Flight Center, Greenbelt, MD, USA

**Abstract** Nonmigrating tides excited in the tropical troposphere by latent heat release from deep convection are known to be responsible for introducing the longitudinal structures in the upper atmosphere and the ionosphere. This study presents for the first time an extensive analysis of the prominent wave-3 and wave-4 longitudinal structures using nearly 14 years of temperature observations by the Microwave Limb Sounder instrument operated on the Aura satellite from 2004 to 2017. The observations reveal significant intraseasonal (~30–60 days) periodic variations in the amplitudes of these wave structures at ~97-km altitude near the mesopause. Some large wave amplitudes accompany strong activity of the Madden-Julian Oscillation. Rainfall data from the Tropical Rainfall Measuring Mission are used as a proxy of latent heating to investigate the source of these variations. Intraseasonal signatures in the wave structures are observed to coincide with the rainfall variations, indicating that the tropospheric 30- to 60-day oscillation is an important driver of the same periodic changes in the upper atmosphere. Given that not all intraseasonal oscillations in the lower atmosphere have corresponding signatures in the longitudinal wave structures, the atmospheric conditions and other influences are important. This study provides evidence on the connection between intraseasonal variations of tides in the upper atmosphere and the changes in the forcing by latent heat release in the troposphere.

## 1. Introduction

Solar thermal tides are global-scale oscillations in atmospheric fields such as density, pressure, temperature, and wind, with integer longitudinal wavenumbers and periods that are harmonics of the Earth's rotation period. By convention they are represented in the form

$$A_{n,s}\cos\left(n\Omega t + s\lambda - \phi_{n,s}\right) \tag{1}$$

where $A$ is the amplitude, $n$ is the harmonic of the planetary rotation period ($n$ = 1, 2, 3, ... represent oscillations with periods of 24, 12, and 8 hr, … and hence are referred to as diurnal, semidiurnal, terdiurnal tides, ...), $\Omega$ is the planetary rotation rate, $t$ is universal time, $s$ is the longitudinal zonal wavenumber ($s$ = 0, ±1, ±2, ±3, …, where $s = 0$ corresponds to standing oscillation, $s > 0$ corresponds to westward propagation, and $s < 0$ corresponds to eastward propagation), $\lambda$ is longitude (positive east), and $\phi$ is the phase; both $A$ and $\phi$ depend on altitude and latitude (e.g., Forbes et al., 2003).

The relation between ground- and space-based observations of atmospheric tides has been explored in previous studies (e.g., Forbes et al., 2006, 2008). Satellite observations are often made from fixed local time perspectives, and it is thus useful to rewrite equation (1) in terms of local time ($t_{LT}$), where it becomes

$$A_{n,s}\cos\left[n\Omega t_{LT} + (s-n)\lambda - \phi_{n,s}\right] \tag{2}$$

In the fixed local time reference frame, tides appear to have longitudinal wavenumbers given by $|s\text{-}n|$. For components with $s = n$, they are longitude independent (and zonally symmetric) and have the zonal phase speed equal to $-\Omega$. When observed by a ground observer, these tides propagate westward at the same speed as the apparent motion or migration of the Sun. The Sun-synchronous tides are referred to as *migrating* tides. The $s \neq n$ longitude-dependent (zonally asymmetric) components are called *nonmigrating* tides. The nonmigrating tides can travel opposite to the Sun's apparent motion or travel faster than the Sun in the same direction.

Tides are often denoted in shorthand notations, combining the rotation periodic harmonic $n$ written as D (diurnal), S (semidiurnal), or T (terdiurnal); the propagation direction written as W (westward) and E

(eastward); and the absolute zonal wavenumber $s$ (e.g., Forbes et al., 2006). For example, DE2 denotes the diurnal tide propagating eastward with zonal wavenumber 2. In the fixed local time reference frame, DE2 tides would produce a longitudinal wavenumber-3 structure ($n$ = 1, $s$ = −2, and $|s\text{-}n|$ = 3). Migrating tides include DW1, SW2, and TW3, and all other tides are defined as nonmigrating tides.

It is now well known that atmospheric tides play an important role in driving large variations in the mesosphere and lower thermosphere (MLT) and the ionosphere (e.g., England et al., 2006; Forbes et al., 2006; Forbes & Wu, 2006; Forbes et al., 2008; Hagan et al., 2007; Liu, 2016; Liu et al., 2010a, 2010b; Oberheide et al., 2006; Pedatella & Forbes, 2009; Talaat & Lieberman, 1999; Warner & Oberheide, 2014; Zhang et al., 2006). These tidal waves are produced in the lower atmosphere, and they can propagate upward into higher altitudes. With increasing altitude and decreasing atmospheric density, the amplitudes of tides grow exponentially. Many tides reach their maximum amplitudes in the MLT region (~80- to 150-km altitude), where they suffer molecular viscous dissipation, depositing momentum and energy they carry into the mean flow and thus modifying the mean circulation in this region (e.g., Forbes et al., 2008).

Nonmigrating tides are mostly excited by latent heat release from tropospheric deep convection (e.g., Forbes et al., 2008). Due to long vertical wavelengths, some nonmigrating tides can propagate through the mesopause and reach the ionosphere $E$ region (~100- to 170-km altitude; e.g., Hagan & Forbes, 2002, 2003), where they modify the wind dynamo and hence cause the longitudinal variations in the $F$ region (e.g., England, 2012; Forbes et al., 2008; Hagan et al., 2007; Immel et al., 2006). DE2 and DE3 are the prominent nonmigrating tides (e.g., Forbes et al., 2008; Warner & Oberheide, 2014). Both tides propagate eastward, and they can modulate the dynamo-generated electric fields and lead to the wave-3 and wave-4 longitudinal structures in the equatorial ionosphere.

Studies have shown that DE2 tides achieve their maximum amplitudes in April–July and November–January, and DE3 amplitudes maximize in August–September, and both tides exhibit significant interannual variability in the MLT region (e.g., Forbes et al., 2008; Oberheide et al., 2006). The interannual variability has been correlated with the El Niño–Southern Oscillation, which produces large changes in precipitation and latent heating (e.g., Lieberman et al., 2007; Pedatella & Liu, 2012, 2013; Warner & Oberheide, 2014). The quasi-biennial oscillation also modulates the tides, and DE2 and DE3 tides are observed to be weaker/stronger during the easterly/westerly phase of the quasi-biennial oscillation (e.g., Wu et al., 2008). Short-term variability has been observed on scales from day-to-day to month (e.g., Forbes et al., 2008; Liu et al., 2010a, 2010b). The day-to-day variability of DE3 is closely related to the variations in tropical rainfall (Miyoshi, 2006). In addition, the interactions between tides and planetary waves (with periods on order of days; e.g., Liu, 2016; Pancheva et al., 2006) have been observed. When planetary waves modulate the amplitudes of tides, the result of such a process is a signature that can have a longitudinal structure associated with the tides and a temporal periodicity associated with those planetary waves (e.g., Liu et al., 2010a, 2010b).

Intraseasonal (~30–90 days) variability has been identified in zonal wind and temperature observations in the MLT region (e.g., Davis et al., 2012; Eckermann et al., 1997; Eckermann & Vincent, 1994; Forbes et al., 2009; Isoda et al., 2004; Lieberman, 1998; Rao et al., 2009; Vergados et al., 2018). Although the intraseasonal cycles in deep convection characterized as the Madden-Julian Oscillation (MJO) (Madden & Julian, 1971) are confined in the lower atmosphere (e.g., Tian et al., 2012; Zhang, 2005), they could modulate the upward propagating nonmigrating tides and gravity waves (Eckermann et al., 1997; Lieberman, 1998) and thus potentially induce the same periodic signatures across a broad range of vertical levels. Indeed, Gasperini et al. (2017) have reported an ~90-day oscillation in zonal mean winds and DE3 tides at ~200- to 400-km altitudes in the thermosphere. Their study uses the Challenging Minisatellite Payload (CHAMP) and Gravity Field and Steady State Ocean Circulation Explorer (GOCE) satellite observations of cross-track winds for 2 years from 2009 to 2010 and identifies the occurrences of persistent 90-day oscillations during the time intervals of intense MJO activity over the given years. However, a rigorous study of a long-term data set has not been conducted, and the intraseasonal cycles in nonmigrating tides in the MLT region have not been extensively studied. The MLT region is the pathway through which the tropospheric impacts must propagate, and a study including both the lower atmosphere and the upper atmosphere is needed in order to establish whether the upper atmosphere variation is connected to the MJO.

In order to fill this knowledge gap, we here perform an extensive analysis of ~14 years of temperature observations by the Microwave Limb Sounder (MLS) instrument operated on the Aura satellite from 2004 to 2017.

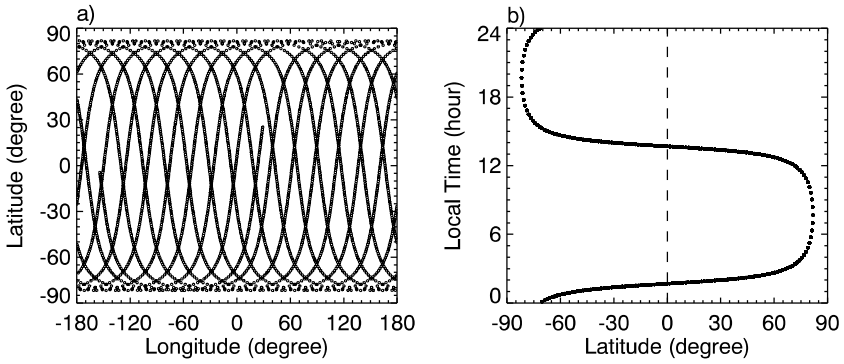


**Figure 1.** Microwave Limb Sounder data coverage for 1 day on 3 January 2016, presented versus longitude and latitude in (a) and latitude and local time in (b). For each day, about 15 longitudes are sampled at fixed local times on the ascending and descending portions of the orbit. Over the equator, the samplings are made at ~1.7 and 13.7 hr separated by 12 hr.

Specifically, the amplitudes of wave-3 and wave-4 longitudinal structures associated with nonmigrating tides at ~97-km altitude are computed, and their ~30- to 60-day periodic signatures are identified over all years. Connections of these periodicities to the intraseasonal forcing in the lower atmosphere are studied using concurrent data of rainfall from the Tropical Rainfall Measuring Mission (TRMM) and the solar f10.7 cm flux. This study allows us to examine and assess the importance of deep convection in affecting the intraseasonal variations of nonmigrating tides in the equatorial MLT region.

## 2. Data and Methods

The Aura satellite is in a near-polar and Sun-synchronous orbit. Owing to the Earth's rotation and the satellite orbit period, about 15 longitudes are observed each day at fixed local times on the ascending and descending portions of the orbit (see Figure 1). As shown, the local time differs by 12 hr between the two orbit portions over the equator, and the local time differences slightly change at higher latitudes. For this study, data are chosen between ±50° latitude, a region where the data coverage is almost continuous in both universal time and longitude.

The Aura/MLS data analyzed here are obtained from the level 2 version 4 temperature product, covering the time interval from July 2004 to December 2017 (available at https://disc.gsfc.nasa.gov). Temperatures are measured at pressure levels ranging from $10^3$ to $10^{-3}$ hPa, corresponding to altitudes from the surface to ~96.7 km in the standard atmosphere. The vertical resolution of the data is about 5 km in the MLT region, and the precision is ~2.5 K (Schwartz et al., 2008). We have used the temperature data at the highest level of 0.001 hPa near the mesopause, where DE2 and DE3 tides are believed to have large amplitudes.

Data from the ascending and descending orbits are separately binned into 5° latitude and 24° longitude intervals for every 5 days (incremented by 1 day) throughout the data set. The number of data points in one bin increases ($>$15) by combining multiple days. For each bin, the temperature differences are calculated (and divided by 2) between the ascending and descending orbits. These measurements are made 12 hr apart in local time, so the differences cancel out the contributions from 12-hr tides and zonal means (they are measured at the same phases by the two orbit portions) but preserve the 24-hr diurnal tide signatures. For each latitude band, a least squares fit to zonal wavenumber 0–4 is then performed to determine the amplitude of each component. Higher wavenumbers are not included as they have small amplitudes and are thus not important to the MLT variations (e.g., Forbes et al., 2008).

The zonal wave 3 and wave 4 from the ascending and descending temperature differences should mostly represent the DE2 and DE3 tides, respectively (e.g., Gasperini et al., 2017; Oberheide & Gusev, 2002). There are also contributions from the DW4 and DW5 tides although their amplitudes are much smaller (e.g., Forbes et al., 2008). Moreover, Lieberman et al. (2006) have examined the vertical phase structure of a given wavenumber from the ascending and descending temperature differences. Their study shows that the phase both increases and decreases with altitude, suggesting the combination of westward and eastward propagations. The propagation directions are thus not determined in this study, and we focus on the wave-3 and wave-4 structures and their periodic variations.

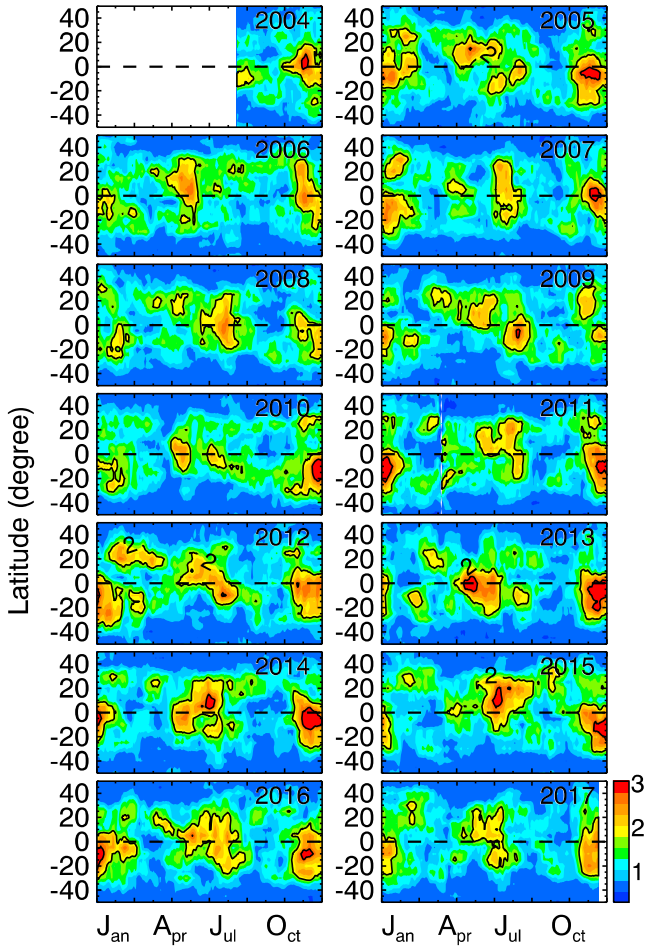


**Figure 2.** Amplitudes of the wave-3 structures observed by Microwave Limb Sounder at ~97-km altitude from August 2004 to December 2017. Here the running 27-day averaged values are presented.

The amplitudes of wave-3 and wave-4 are averaged using the 27-day running window stepped by 1 day to remove short-scale variability. This running average also removes variations that could potentially be caused by the 27-day solar rotation cycle. To investigate the possible presence of intraseasonal periodicities, the periodogram of the wave amplitudes is calculated employing the Lomb-Scargle method (e.g., Lomb, 1976; Scargle, 1982). For this study, the spectra are computed using the 180-day running window stepped by 1 day throughout the series of wave amplitudes. This 180-day window allows for determining periodicities between 30 and 60 days with acceptable sampling and spectral resolutions, and the running window enables identifying the time intervals when the periodicities occur. Occurrences of these intraseasonal periodic variations are compared with those of latent heating in the troposphere.

The MJO activity can be represented by the Real-time Multivariate MJO (RMM) index that has been widely used in the research community (e.g., Tian et al., 2012; Waliser et al., 2009). The index is a pair of principal component time series based upon the multivariate empirical orthogonal functions (e.g., Waliser et al., 2009; Wheeler & Hendon, 2004). Values of RMM are available throughout the same time interval as the MLS observations (at http://www.bom.gov.au). Strong MJO activity are considered to occur when RMM $>$ 1.

The 3B42 precipitation data from TRMM (Huffman et al., 2007) are used as a proxy for latent heat release associated with deep convection. Rainfall rates have been provided for every 3 hr, covering between ±50° latitude and at all longitudes (at 0.25° × 0.25° latitude/longitude grids). These data are available for the entire time interval considered here (https://disc.gsfc.nasa.gov). For this study, the rainfall data at each 3 hr are averaged over the equator (±5° latitude) and binned into 24° longitude intervals. A 2D-FFT (Fast Fourier Transform) is applied to these data within the 5-day running window (stepped by 1 day) to calculate the amplitudes of diurnal (24-hr period) E2 (propagate eastward with zonal wavenumber 2) and E3 (propagate eastward with zonal wavenumber 3) components that are expected to excite the DE2 and DE3 tides. Occurrences of 30- to 60-day periodicities in these components are studied throughout the data set.

The daily f10.7 cm solar fluxes (available at https://omniweb.gsfc.nasa.gov) are used to investigate their possible influences on the mesospheric variations. The periodogram is calculated based upon the 27-day running averaged solar fluxes, and the solar cycle variation with periods of 10.28 and 7.86 years has been removed. The 30- to 60-day periodicities are screened through the entire time interval studied.

## 3. Results and Discussion

Figure 2 presents the amplitudes of wave-3 structures from the MLS temperature measurements at the vertical level of ~97 km, as a function of time (for all years from 2004 to 2017) and latitude. Clearly, the waves have their largest amplitudes in the equatorial region between ±30° latitudes, with a seasonal and interannual pattern. The amplitude has peaks around April–July in Northern Hemisphere and from November–January in Southern Hemisphere. During 2011–2015, the peaks are stronger and shift to center near the equator, exhibiting a variation that might relate to the solar cycle. These signatures have been reported before for the DE2 tides (e.g., Forbes et al., 2008; Oberheide et al., 2006).

By comparison, the wave-4 structures (Figure 3) are observed to have larger amplitudes with the largest value of ~6 K, being about a factor of 2 greater than wave-3. This is reasonable as the DE3 tides normally have larger amplitudes than the DE2 (e.g., Forbes et al., 2008). The wave-4 structures are centered around the equator within ±20° latitude, also showing identifiable seasonal patterns. The amplitudes maximize around

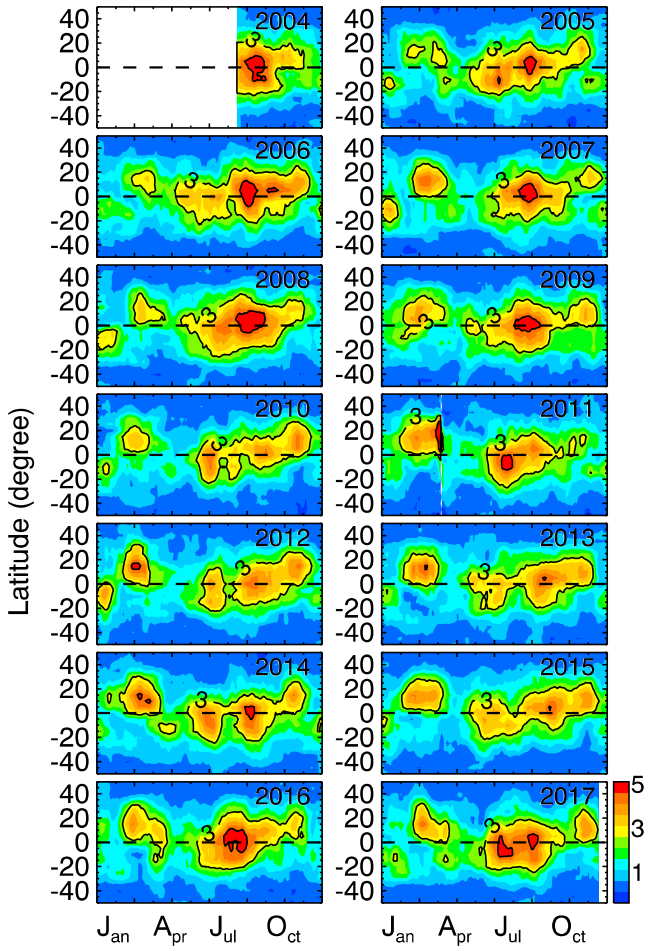


**Figure 3.** Same as Figure 2 but for the wave-4 structures.

August–September, being consistent with the DE3 signatures reported before by previous studies (e.g., Oberheide et al., 2011). Away from the equator, there are large amplitude values in January in SH and February/March in NH.

The latitudinal structures are rather similar between wave-3 and wave-4 as they both show symmetrical features around the equator. As discussed by Forbes et al. (2008), this symmetry suggests that higher-order and short-wavelength waves comprising the tides tend to dissipate, leaving symmetric waves to propagate upward into upper levels. However, wave-3 can extend to ±30° latitude, while wave-4 is more important within ±20° latitude. This larger latitude range suggests that the DE2 tides are more efficient in generating dynamo electric fields in the *E* region (e.g., Forbes et al., 2008).

Figure 4a shows the time series of wave-3 amplitudes at the equator for all years from 2004 to 2017, and Figure 4b shows the running periodogram of these amplitudes. Significant oscillations (above 95% confidence level) with periods between 30 and 60 days (on intraseasonal scales) are recognizable over certain time intervals. Longer period variations are also observed in the periodogram, but they are not the focus of this study. The wave amplitudes have been smoothed through the 27-day running averaging, so shorter-scale periodicities ($<$27 days) are not visible. The intraseasonal variations occur in episodes, showing their intermittent signature. Each episode lasts for many days, suggesting the long lifetimes of these intraseasonal oscillations.

Similarly, Figure 5 presents the equatorial values of the wave-4 amplitudes and the running periodogram for the entire data set. Again, periodic 30- to 60-day oscillations are noticed in the periodogram above the statistically significant level. Each burst of periodic oscillation is observed to last over many days. These wave signatures are consistent with those seen in wave-3. In what follows, the 30- to 60-day variations are studied in comparison with the intraseasonal signatures of the potential driver of latent heating.

The time series in Figures 4a and 5a also show that there are large amplitudes in wave-3 and wave-4 during strong MJO activity represented by the RMM index (strong MJO occurs at RMM $>$ 1). The MJO is the dominant intraseasonal forcing in the lower atmosphere, and it is characterized as the large-scale movement of deep convection and precipitation (e.g., Tian et al., 2012; Zhang, 2005). Given that excitations of DE2 and DE3 tides are largely affected by latent heating from deep convection, the intraseasonal periodicities in latent heating are explored.

Figure 6 presents the diurnal E2 components of the tropical rainfall from TRMM and the running periodogram using the 180-day window stepped by 1 day throughout 2004–2017. Periodic signatures between 30 and 60 days are noticeable in the periodogram, and they occur at time intervals covering many days. Here the rainfall components have been averaged through the 27-day running window, so shorter-scale periodicities are filtered. The intraseasonal variations also occur on episodes, exhibiting their intermittent signature. Compared with Figure 4, the rainfall variations are observed at more time intervals than the wave-3, and the time intervals extend to cover more days. These indicate that the intraseasonal forcing of rainfall occurs more often and lasts longer than the response in the upper atmosphere. The upward propagations of tides from the source region into higher levels are largely affected by the background atmospheric conditions; it is thus reasonable that the wave-3 does not always respond to the rainfall.

Figure 7 presents the diurnal E3 components of rainfall in the same way. Large 30- to 60-day periodicities of these components are observed, and they occur at time intervals for many days. Longer-periodic variations are not considered as this study is concerned with the intraseasonal periodicities. Compared to Figure 5, the intraseasonal forcing of rainfall also occurs more often and lasts longer than the wave-4.

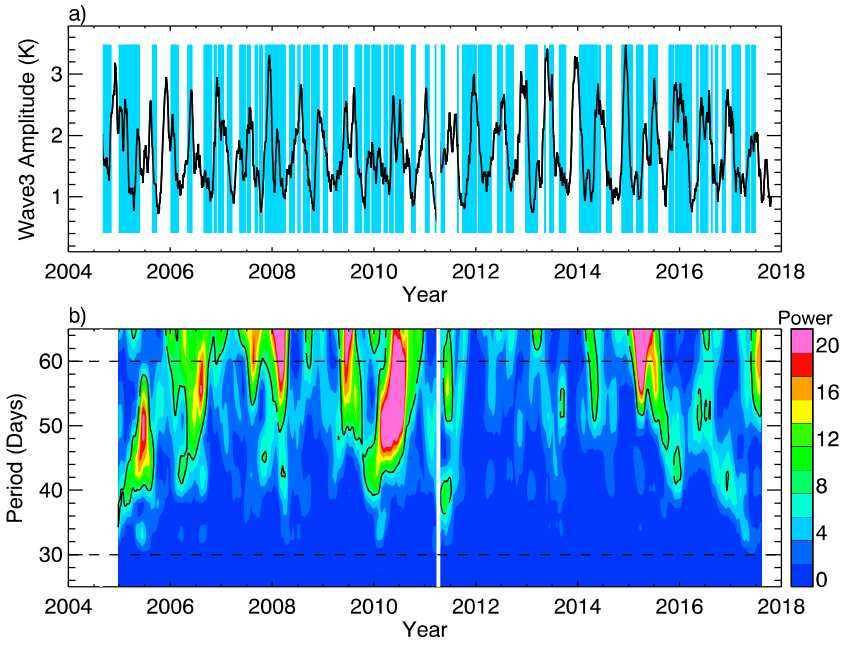


**Figure 4.** (a) Time series of the 27-day running averaged wave-3 amplitudes at the equator (in black) during August 2004 to December 2017. Madden-Julian Oscillation (MJO) episodes with Real-time Multivariate MJO $>$ the 50th percentile (=1.2) are highlighted in blue color. (b) Running Lomb-Scargle periodogram of the wave-3 amplitude based upon the 180-day running window stepped by 1 day. The black contour lines mark the 95% confidence levels.

Figure 8 shows the time series of the 27-day averaged f10.7 cm solar fluxes and the periodogram throughout 2004–2017. As these are averaged values, only periodicities $>$27 days are present. Large spectrum powers corresponding to 30- to 60-day periodicities are observed. It can be seen that the solar flux also exhibits the same periodic signatures as the wave-3 and wave-4 amplitudes.

Figure 9 compares the occurrences of intraseasonal variations in wave-3 and wave-4 in relation to the tropospheric latent heating. The figure includes all time intervals for which the 30- to 60-day periodic

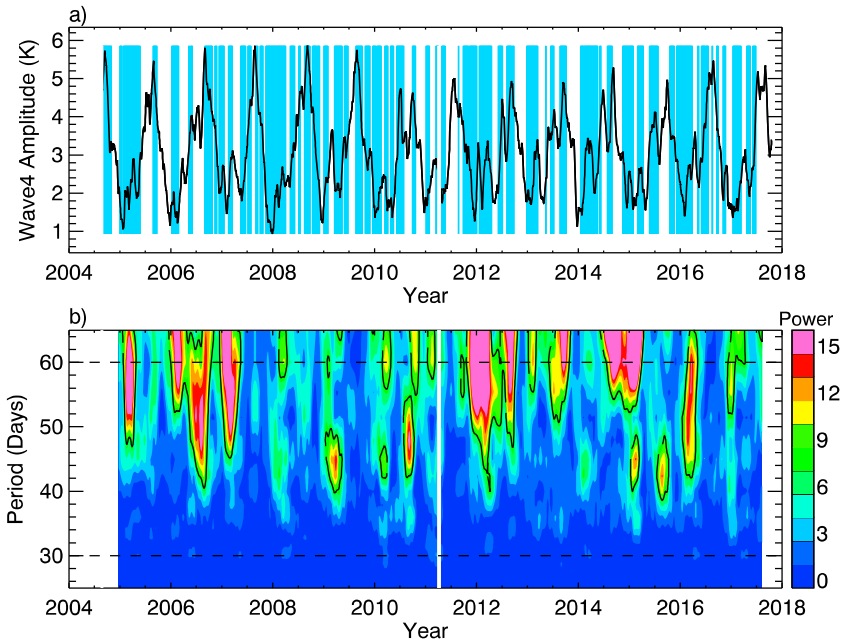


**Figure 5.** Same as Figure 4 but for the wave-4 structures.

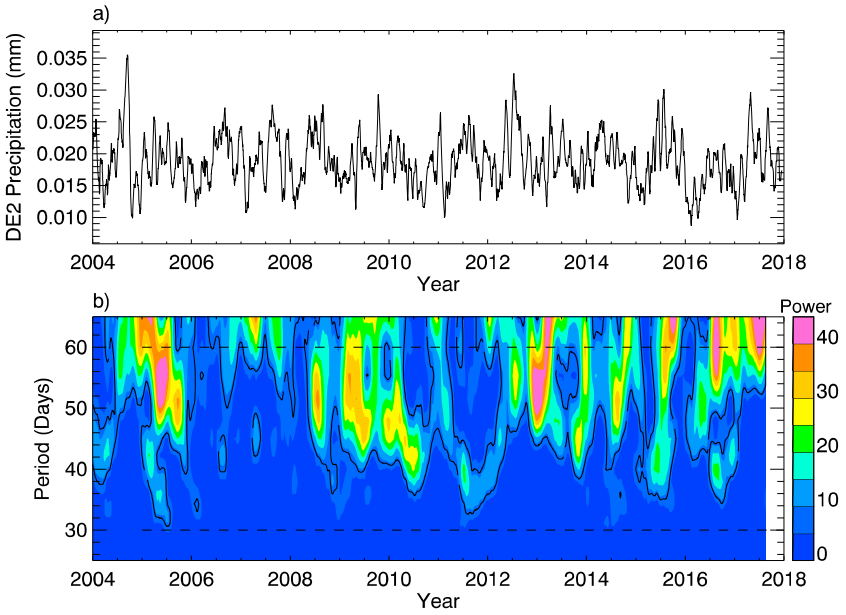


**Figure 6.** (a) Time series and (b) running Lomb-Scargle periodogram of the diurnal E2 component of the tropospheric rainfall from the Tropical Rainfall Measuring Mission data over the equator for all years from 2004 to 2017.

signatures are observed throughout the 13 years presented from 2005 to 2017. Over these time intervals, the periodograms exhibit significant (>95% confidence levels) variations with the periods between 30 and 60 days. As illustrated, the intraseasonal signatures are recognizable at 9 time intervals for wave-3 (black bars) and 9 intervals for diurnal E2 rainfall (blue bars) in Figure 9a, and there are 11 intervals for wave-4 (black bars) and 9 intervals for diurnal E3 rainfall (blue bars) in Figure 9b. For wave-3 and wave-4, their intraseasonal periodicities have overlaps with the rainfall signatures, suggesting that the wave-3 and wave-4 variations could be affected by the changes of latent heating. However, the rainfall changes are observed to occur over longer time intervals. For some intervals (one of nine intervals in diurnal E2 component and two of nine intervals in diurnal E3), the wave structures are not observed to have the

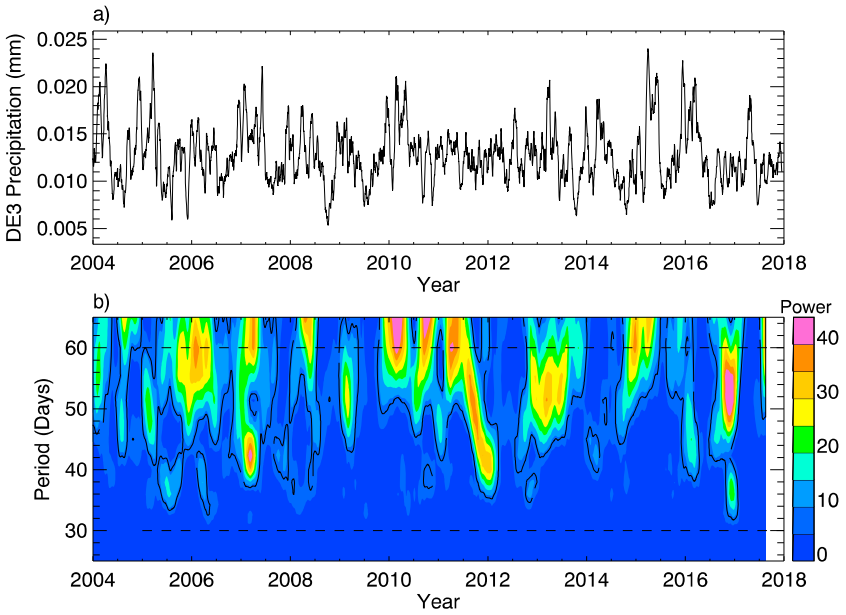


**Figure 7.** Same as Figure 6 but for the diurnal E3 component in rainfall.

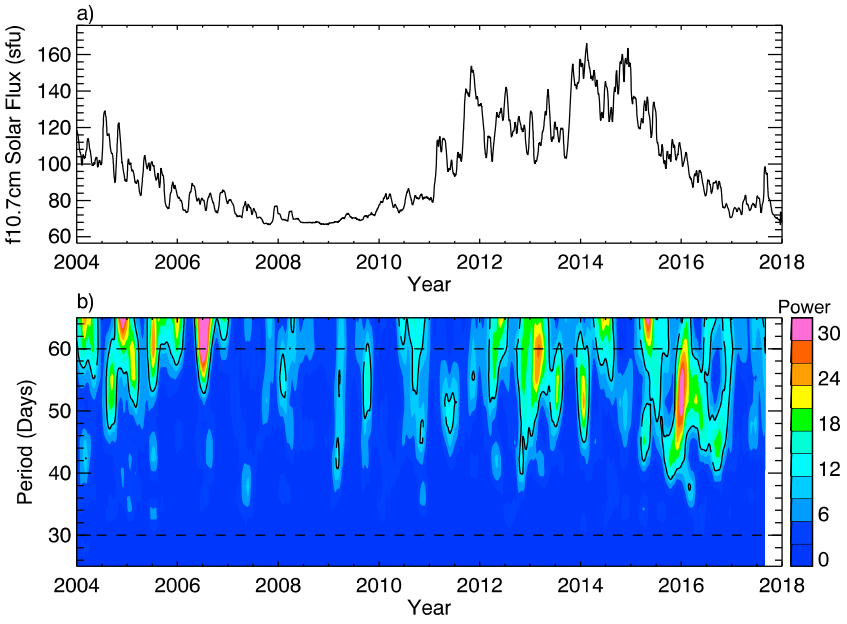


**Figure 8.** (a) Time series and (b) running Lomb-Scargle periodogram of the f10.7 cm solar flux throughout 2004–2017. The solar fluxes presented have been averaged through the 27-day running window.

30- to 60-day periodic signatures. That is, the rainfall variations are not always coincident with the same periodic variations of wave-3 and wave-4. These indicate that not all rainfall changes could cause the correspondent variations in the wave structures. Nonetheless, the intraseasonal cycle of deep convection in the troposphere appears to be important to the 30- to 60-day variation in the longitudinal wave structure near the mesopause.

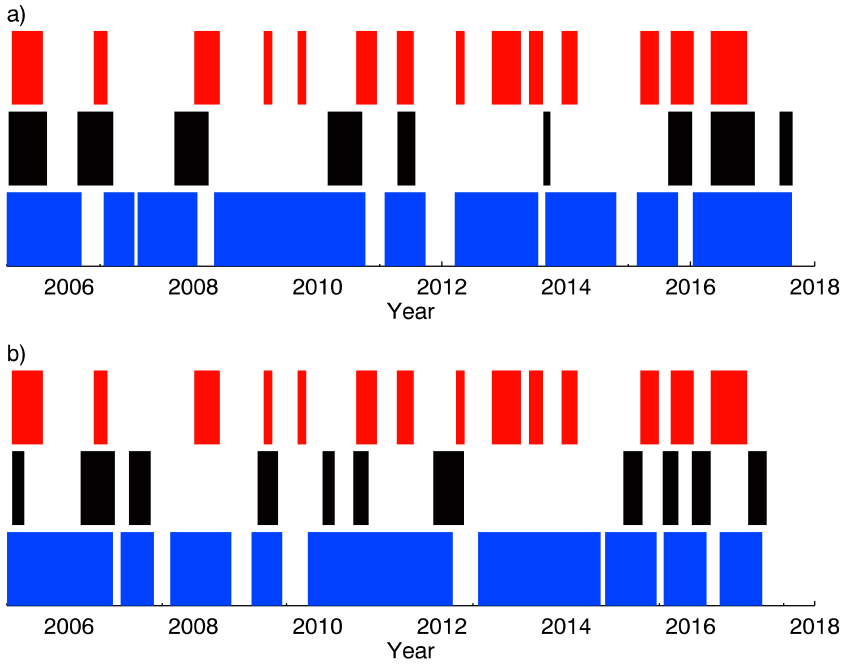


**Figure 9.** Occurrences (time intervals) of 30- to 60-day periodicities in (a) wave-3 and (b) wave-4 longitudinal structures (shown as black bars), in comparison with the 30- to 60-day periodicities of latent heating (shown in blue) and solar forcing (shown in red) during the concurrent data interval from 2005–2017.

The wave-3 and wave-4 longitudinal structures are associated with the nonmigrating tides excited in the troposphere from deep convection. In the presence of intraseasonal cycles, the tidal forcing should have the same periodicities of ~30- to 60-days. It is thus reasonable to observe the intraseasonal signatures in tides and the associated longitudinal wave structures. As the signatures are not always observed in coincidence with the tropospheric cycles, the atmospheric conditions and other influences are in effect. Conditions that are favorable must occur for the intraseasonal cycles in the lower atmosphere to drive the corresponding variations in the upper atmosphere.

In addition, tides could interact strongly with longer-period waves and such an interaction would result in a signature that has the longitudinal wave structures associated with the tides and the periodicities associated with the longer-period waves (e.g., Liu, 2016; Pancheva et al., 2006). This study identifies the wave-3 and wave-4 longitudinal structures and their 30- to 60-day periodicities in the MLT region. It is believed that the MJO cannot propagate into the mesosphere, whereas tides can. Thus, it may be expected that the intraseasonal cycles of the troposphere interact with the DE2 and DE3 tides and the ~30- to 60-day periodicities are carried into higher altitudes.

Nonmigrating tides are known to be able to propagate through the mesopause, modulating dynamo electric fields and producing the longitudinal structures in the ionosphere (e.g., Forbes et al., 2008; Immel et al., 2006). The wave-3 and wave-4 tidal structures are thus expected to carry the periodic signatures upward and produce the intraseasonal variability in both the *E* and *F* region ionosphere. However, further analyses are needed in order to understand both the causes of the intraseasonal variability of tides and how exactly these may accordingly produce the variations in the MLT region and the ionosphere.

The relation between the tidal wave variations and the solar forcing is also illustrated in Figure 9. In total, there are 14 time intervals at which the intraseasonal signatures are seen in the solar flux. Not all intervals overlap with the tidal variations, which supports the hypothesis that the intraseasonal variation in the MLT region is not directly driven by the solar irradiance. For many cases (eight in wave-3 and seven in wave-4), the 30- to 60-day periodicities coincide with the solar flux variations, indicating that these structures are largely affected by the solar irradiance. Both the solar flux variations and those of the atmosphere exhibit intraseasonal signatures, and this similarity suggests that the Sun should be the source of both variations given that the Sun is independent with the atmosphere. The DE2 and DE3 tides are excited in the lower atmosphere, and their variations are observed to relate to the atmosphere. The solar influence on the wave-3 and wave-4 structures could thus arise from the impact on the troposphere or by simply influencing the temperature of the lower atmosphere directly. The solar influence appears to be broad, and the 30- to 60-day periodicities of wave-3 and wave-4 are observed at less time intervals. This indicates that the upper atmosphere does not always respond to the Sun, and conditions of the background atmosphere and other influences are also important. However, the solar forcing is not the focus of the current study and a further study is needed in order to explain this relation.

## 4. Summary and Conclusions

This study reports an extensive analysis of ~14 years of temperature observations of longitudinal wave-3 and wave-4 structures associated with nonmigrating tides in the MLT region by Aura/MLS from 2004 to 2017. Intraseasonal variations with periods between 30 and 60 days are recognized in the amplitudes of these structures. Their connection to the lower atmosphere forcing is explored using the concurrent rainfall data from TRMM and the f10.7 cm solar flux data. The analysis suggests that the intraseasonal cycles induced by changing latent heating from deep convection in the troposphere could extend their influences into higher altitudes and cause corresponding variations near the mesopause.

In this study, all time intervals with 30- to 60-day periodic signatures are identified throughout the data sets studied. The variations in wave-3 and wave-4 are observed coincident with the same periodic signatures in latent heating, showing that the tropospheric forcing is an important driver of the upper atmosphere variations. Not all tropospheric oscillations are observed at the same times as the variations of the longitudinal structures, suggesting that the atmospheric conditions and other influences are important. Given that the tropospheric cycles concur with the tidal wave variations, the favored conditions for the tropospheric forcing to affect the MLT region occur. Furthermore, the intraseasonal signatures are observed in solar flux, indicating that the solar irradiance is also important to produce the variations in the MLT region.

**Acknowledgments**
The Aura/MLS level 2 version 4 temperature data and the TRMM 3B42 precipitation data are publicly available at https://disc.gsfc.nasa.gov. The MJO RMM index data are available at http://www.bom.gov.au. The solar flux data are available at https://omniweb.gsfc.nasa.gov. The authors thank the providers of data used in the present study. This work was supported by the NASA/TIMED project and the NASA grant. Government sponsorship is acknowledged.

## References

Davis, R. N., Chen, Y.-W., Miyahara, S., & Mitchell, N. J. (2012). The climatology, propagation and excitation of ultra-fast Kelvin waves as observed by meteor radar, Aura MLS, TRMM and in the Kyushu-GCM. *Atmospheric Chemistry and Physics*, *12*(4), 1865–1879. https://doi.org/10.5194/acp-12-1865-2012

Eckermann, S. D., Dajopadhyaya, D. K., & Vincent, R. A. (1997). Intraseasonal wind variability in the equatorial mesosphere and lower thermosphere: Long-term observations from the central Pacific. *Journal of Atmospheric and Solar - Terrestrial Physics*, *59*(6), 603–627. https://doi.org/10.1016/S1364-6826(96)00143-5

Eckermann, S. D., & Vincent, R. A. (1994). First observations of intraseasonal oscillations in the equatorial mesosphere and lower thermosphere. *Geophysical Research Letters*, *21*(4), 265–268. https://doi.org/10.1029/93GL02835

England, S. L. (2012). A review of the effects of non-migrating atmospheric tides on the Earth's low-latitude ionosphere. *Space Science Reviews*, *168*(1-4), 211–236. https://doi.org/10.1007/s11214-011-9842-4

England, S. L., Maus, S., Immel, T. J., & Mende, S. B. (2006). Longitudinal variation of the E-region electric fields caused by atmospheric tides. *Geophysical Research Letters*, *33*, L21105. https://doi.org/10.1029/2006GL027465

Forbes, J. M., Russell, J., Miyahara, S., Zhang, X., Palo, S., Mlynczak, M., et al. (2006). Troposphere-thermosphere tidal coupling as measured by the SABER instrument on TIMED during July–September 2002. *Journal of Geophysical Research*, *111*, A10S06. https://doi.org/10.1029/2005JA011492

Forbes, J. M., & Wu, D. (2006). Solar tides as revealed by measurements of mesospheric temperature by the MLS experiment on UARS. *Journal of the Atmospheric Sciences*, *63*(7), 1776–1797. https://doi.org/10.1175/JAS3724.1

Forbes, J. M., Zhang, X., Palo, S., Russell, J., Mertens, C. J., & Mlynczak, M. (2008). Tidal variability in the ionospheric dynamo region. *Journal of Geophysical Research*, *113*, A02310. https://doi.org/10.1029/2007JA012737

Forbes, J. M., Zhang, X., Palo, S. E., Russell, J., Mertens, C. J., & Mlynczak, M. (2009). Kelvin waves in stratosphere, mesosphere and lower thermosphere temperatures as observed by TIMED/SABER during 2002-2006. *Earth, Planets and Space*, *61*(4), 447–453. https://doi.org/10.1186/BF03353161

Forbes, J. M., Zhang, X., Talaat, E. R., & Ward, W. (2003). Nonmigrating diurnal tides in the thermosphere. *Journal of Geophysical Research*, *108*(A1), 1033. https://doi.org/10.1029/2002JA009262

Gasperini, F., Hagan, M. E., & Zhao, Y. (2017). Evidence of tropospheric 90 day oscillations in the thermosphere. *Geophysical Research Letters*, *44*, 10,125–10,133. https://doi.org/10.1002/2017GL075445

Hagan, M. E., & Forbes, J. M. (2002). Migrating and nonmigrating diurnal tides in the middle and upper atmosphere excited by tropospheric latent heat release. *Journal of Geophysical Research*, *107*(D24), 4754. https://doi.org/10.1029/2001JD001236

Hagan, M. E., & Forbes, J. M. (2003). Migrating and nonmigrating semidiurnal tides in the upper atmosphere excited by tropospheric latent heat release. *Journal of Geophysical Research*, *108*(A2), 1062. https://doi.org/10.1029/2002JA009466

Hagan, M. E., Maute, A., Roble, R. G., Richmond, A. D., Immel, T. J., & England, S. L. (2007). Connections between deep tropical clouds and the Earth's ionosphere. *Geophysical Research Letters*, *34*, L20109. https://doi.org/10.1029/2007GL030142

Huffman, G. J., Adler, R. F., Bolvin, D. T., Gu, G. J., Nelkin, E. J., Bowman, K. P., et al. (2007). The TRMM multisatellite precipitation analysis (TMPA): Quasi-global, multiyear, combined-sensor precipitation estimates at fine scales. *Journal of Hydrometeorology*, *8*(1), 38–55. https://doi.org/10.1175/JHM560.1

Immel, T. J., Sagawa, E., England, S. L., Henderson, S. B., Hagan, M. E., Mende, S. B., et al. (2006). Control of equatorial ionospheric morphology by atmospheric tides. *Geophysical Research Letters*, *33*, L15108. https://doi.org/10.1029/2006GL026161

Isoda, F., Tsuda, T., Nakamura, T., Vincent, R. A., Reid, I. M., Achmad, E., et al. (2004). Intraseasonal oscillations of the zonal wind near the mesopause observed with medium-frequency and meteor radars in the tropics. *Journal of Geophysical Research*, *109*, D21108. https://doi.org/10.1029/2003JD003378

Lieberman, R. S. (1998). Intraseasonal variability of high-resolution Doppler imager winds in the equatorial mesosphere and lower thermosphere. *Journal of Geophysical Research*, *103*(D10), 11,221–11,228. https://doi.org/10.1029/98JD00532

Lieberman, R. S., Riggin, D. M., Garcia, R. R., Qu, Q., & Remsberg, E. E. (2006). Observations of intermediate-scale diurnal waves in the equatorial mesosphere and lower thermosphere. *Journal of Geophysical Research*, *111*, A10S11. https://doi.org/10.1029/2005JA011498

Lieberman, R. S., Riggin, D. M., Ortland, D. A., Nesbitt, S. W., & Vincent, R. A. (2007). Variability of mesospheric diurnal tides and tropospheric diurnal heating during 1997-1998. *Journal of Geophysical Research*, *112*, D20110. https://doi.org/10.1029/2007JD008578

Liu, G., Immel, T. J., England, S. L., Kumar, K. K., & Ramkumar, G. (2010a). Temporal modulations of the longitudinal structure in $F_2$ peak height in the equatorial ionosphere as observed by COSMIC. *Journal of Geophysical Research*, *115*, A04303. https://doi.org/10.1029/2009JA014829

Liu, G., Immel, T. J., England, S. L., Kumar, K. K., & Ramkumar, G. (2010b). Temporal modulations of the four-peaked longitudinal structure of the equatorial ionosphere by the 2 day planetary wave. *Journal of Geophysical Research*, *115*, A12338. https://doi.org/10.1029/2010JA016071

Liu, H.-L. (2016). Variability and predictability of the space environment as related to lower atmosphere forcing. *Space Weather*, *14*, 634–658. https://doi.org/10.1002/2016SW001450

Lomb, N. R. (1976). Least-squares frequency analysis of unequally spaced data. *Astrophysics and Space Science*, *39*(2), 447–462. https://doi.org/10.1007/BF00648343

Madden, R. A., & Julian, P. R. (1971). Detection of a 40-50 day oscillation in the zonal wind in the tropical Pacific. *Journal of the Atmospheric Sciences*, *28*(5), 702–708. https://doi.org/10.1175/1520-0469(1971)028<0702:DOADOI>2.0.CO;2

Miyoshi, Y. (2006). Temporal variation of nonmigrating diurnal tide and its relation with the moist convective activity. *Geophysical Research Letters*, *33*, L11815. https://doi.org/10.1029/2006GL026072

Oberheide, J., Forbes, J. M., Zhang, X., & Bruinsma, S. L. (2011). Climatology of upward propagating diurnal and semidiurnal tides in the thermosphere. *Journal of Geophysical Research*, *116*, A11306. https://doi.org/10.1029/2011JA016784

Oberheide, J., & Gusev, O. A. (2002). Observation of migrating and nonmigrating diurnal tides in the equatorial lower thermosphere. *Geophysical Research Letters*, *29*(24), 2167. https://doi.org/10.1029/2002GL016213

Oberheide, J., Qu, Q., Killeen, T. L., Hagan, M. E., & Roble, R. G. (2006). Diurnal nonmigrating tides from TIMED Doppler Interferometer wind data: Monthly climatologies and seasonal variations. *Journal of Geophysical Research*, *111*, A10S03. https://doi.org/10.1029/2005JA011491

Pancheva, D. V., Mukhtarov, P. J., Shepherd, M. G., Mitchell, N. J., Fritts, D. C., Riggin, D. M., et al. (2006). Two-day wave coupling of the low-latitude atmosphere-ionosphere system. *Journal of Geophysical Research*, *111*, A07313. https://doi.org/10.1029/2005JA011562

Pedatella, N. M., & Forbes, J. M. (2009). Interannual variability in the longitudinal structure of the low-latitude ionosphere due to the El Niño–Southern Oscillation. *Journal of Geophysical Research*, *114*, A12316. https://doi.org/10.1029/2009JA014494

Pedatella, N. M., & Liu, H.-L. (2012). Tidal variability in the mesosphere and lower thermosphere due to the El Niño/Southern Oscillation. *Geophysical Research Letters*, *39*, L19802. https://doi.org/10.1029/2012GL053383

Pedatella, N. M., & Liu, H.-L. (2013). Influence of the El Niño Southern Oscillation on the middle and upper atmosphere. *Journal of Geophysical Research: Space Physics*, *118*, 2744–2755. https://doi.org/10.1002/jgra.50286

Rao, R. K., Gurubaran, S., Sathishkumar, S., Sridharan, S., Nakamura, T., Tsuda, T., et al. (2009). Longitudinal variability in intraseasonal oscillation in the tropical mesosphere and lower thermosphere region. *Journal of Geophysical Research*, *114*, D19110. https://doi.org/10.1029/2009JD011811

Scargle, J. D. (1982). Studies in astronomical time series analysis. II. Statistical aspects of spectral analysis of unevenly spaced data. *The Astrophysical Journal*, *263*, 835–853. https://doi.org/10.1086/160554

Schwartz, M. J., Lambert, A., Manney, G. L., Read, W. G., Livesey, N. J., Froidevaux, L., et al. (2008). Validation of the aura microwave limb sounder temperature and geopotential height measurements. *Journal of Geophysical Research*, *113*, D15S11. https://doi.org/10.1029/2007JD008783

Talaat, E. R., & Lieberman, R. S. (1999). Nonmigrating diurnal tides in mesospheric and lower-thermospheric winds and temperatures. *Journal of the Atmospheric Sciences*, *56*(24), 4073–4087. https://doi.org/10.1175/1520-0469

Tian, B., Ao, C. O., Waliser, D. E., Fetzer, E. J., Mannucci, A. J., & Teixeira, J. (2012). Intraseasonal temperature variability in the upper troposphere and lower stratosphere from the GPS radio occultation measurements. *Journal of Geophysical Research*, *117*, D15110. https://doi.org/10.1029/2012JD017715

Vergados, P., Liu, G., Mannucci, A. J., & Janches, D. (2018). Equatorial intraseasonal temperature oscillations in the lower thermosphere from SABER. *Geophysical Research Letters*, *45*. https://doi.org/10.1029/2018GL079467

Waliser, D., Sperber, K., Hendon, H., Kim, D., Maloney, E., Wheeler, M., et al. (2009). MJO simulation diagnostics. *Journal of Climate*, *22*(11), 3006–3030. https://doi.org/10.1175/2008JCLI2731.1

Warner, K., & Oberheide, J. (2014). Nonmigrating tidal heating and MLT tidal wind variability due to the El Niño-Southern Oscillation. *Journal of Geophysical Research: Atmospheres*, *119*, 1249–1265. https://doi.org/10.1002/2013JD020407

Wheeler, M. C., & Hendon, H. H. (2004). An all-season real-time multivariate MJO index: Development of an index for monitoring and prediction. *Monthly Weather Review*, *132*(8), 1917–1932. https://doi.org/10.1175/1520-0493(2004)132<1917:AARMMI>2.0.CO;2

Wu, Q., Ortland, D. A., Killeen, T. L., Roble, R. G., Hagan, M. E., Liu, H.-L., et al. (2008). Global distribution and inter-annual variations of mesospheric and lower thermospheric neutral wind diurnal tide, part 2: Non-migrating tide. *Journal of Geophysical Research*, *113*, A05309. https://doi.org/10.1029/2007JA012543

Zhang, C. (2005). Madden-Julian Oscillation. *Reviews of Geophysics*, *43*, RG2003. https://doi.org/10.1029/2004RG000158

Zhang, X., Forbes, J. M., Hagan, M. E., Russell, J. M. III, Palo, S. E., Mertens, C. J., & Mlynczak, M. G. (2006). Monthly tidal temperatures 20–120 km from TIMED/SABER. *Journal of Geophysical Research*, *111*, A10S08. https://doi.org/10.1029/2005JA011504